IOPscience iopscience.iop.org

Home Search Collections Journals About Contact us My IOPscience

Fundamental measure density functional theory for hard spherocylinders in static and time-dependent aligning fields

This article has been downloaded from IOPscience. Please scroll down to see the full text article.

2010 J. Phys.: Condens. Matter 22 104112

(http://iopscience.iop.org/0953-8984/22/10/104112)

View the table of contents for this issue, or go to the journal homepage for more

Download details:
IP Address: 134.99.64.131
The article was downloaded on 09/06/2010 at 09:49

Please note that terms and conditions apply.

IOP Publishing Journal of Physics: Condensed Matter

J. Phys.: Condens. Matter **22** (2010) 104112 (11pp) doi:10.1088/0953-8984/22/10/104112

# Fundamental measure density functional theory for hard spherocylinders in static and time-dependent aligning fields

**A Härtel and H Löwen**

Institut für Theoretische Physik II: Weiche Materie, Heinrich-Heine-Universität Düsseldorf, Universitätsstraße 1, D-40225 Düsseldorf, Germany

Received 18 September 2009, in final form 30 October 2009
Published 23 February 2010
Online at stacks.iop.org/JPhysCM/22/104112

**Abstract**

The recently developed fundamental measure density functional theory (Hansen-Goos and Mecke 2009 *Phys. Rev. Lett.* **102** 018302) for an inhomogeneous anisotropic hard body fluid is used as a basic ingredient in treating the Brownian dynamics of hard spherocylinders. After discussing the relevance of a free parameter in the fundamental measure density functional for the isotropic–nematic transition in equilibrium, we discuss the equilibrium phase behaviour of hard spherocylinders in a static external potential which couples only to the orientations. For external potentials favouring rod orientations along the poles of the unit sphere, there is a well-known paranematic–nematic transition which ceases to exist above a threshold of the strength $V_0$ of the external potential. However, when orientations along the equator are more favoured, in the plane of the potential energy $V_0$ and density, there is a phase transition from paranematic to nematic for any strength, which becomes second order above a critical threshold of $V_0$. The full equilibrium phase diagram in the $V_0$–density plane is computed for a fixed rod aspect ratio of 5. For the equatorial cases, strength $V_0$ is then oscillating in time and dynamical density functional theory is used to compute the evolution of the orientational distribution. A subtle resonance for increasing oscillation frequencies is detected if the oscillating $V_0$ crosses the paranematic–nematic phase transition.

(Some figures in this article are in colour only in the electronic version)

## 1. Introduction

Classical density functional theory for inhomogeneous fluids constitutes a versatile and unifying approach to freezing [1–6]. The primary interest was first on spherical particles whose interactions are governed by radially symmetric pair potentials. In principle, however, density functional theory is also applicable to anisotropic bodies with an orientational degree of freedom. If the particles are rotationally symmetric with respect to an orientable body axis, both the translational vector pointing to their centres-of-mass and their orientational (unit) vectors are needed to describe a configuration properly.

Density functional theory of freezing has been applied to orientable hard rod-like particles [7, 8] and different stable liquid crystalline phases were obtained as a function of the rod aspect ratio and the particle number density. Most of those were in agreement with computer simulations [9] and cell theory [10, 11]. Also the exact Onsager solution of the isotropic nematic phase in the limit of thin rods can be cast into the density functional language [12] corresponding to an inhomogeneous second-virial expansion.

For the simplest nontrivial interacting system, namely that of hard spheres, Rosenfeld's fundamental measure theory [13] turned out to be a reliable and predictive approach to freezing [6, 14, 15]. Recently the fundamental measure approach was generalized to hard bodies of *arbitrary* shape by Hansen-Goos and Mecke [16]. In particular, the theory was applied to an isotropic phase near hard walls and good agreement was obtained for the inhomogeneous density profiles with simulation data.

For Brownian particles like colloids, the density functional approach was generalized towards *dynamics* in nonequilibrium, e.g. for an imposed time-dependent external potential. One convenient way is to derive it from the Smoluchowski equation [17]. Also for orientational degrees of freedom a dynamical density functional theory was derived

 © 2010 IOP Publishing Ltd Printed in the UK

from the Smoluchowski equation [18] for Brownian rods [19]. Time-dependent situations of an inhomogeneous isotropic phase were considered in [20]. The orientational dynamical density functional theory was also recently applied to self-propelled rods [21].

In this paper, we apply the fundamental measure functional proposed by Hansen-Goos and Mecke [16] to hard spherocylinders in a time-dependent external field which solely couple to the orientational degrees of freedom. The amplitude of this external coupling is oscillating in time. Furthermore we evaluate the fundamental measure approach for the bulk isotropic and nematic phase and discuss thereby the influence of a free parameter in the theory. After having fixed this parameter, we calculate the equilibrium phases in a static external potential which couples only to the orientational degrees of freedom. In particular, if the external potential favours rod orientations along the poles of a unit sphere, there is a first-order paranematic–nematic transition [8, 22] which ceases to exist above a threshold amplitude $V_0$ of the external coupling. If orientations along the equator of the unit sphere are preferred, on the other hand, there is a phase transition from a paranematic to a nematic phase for any strength $V_0$ which gets second order above a critical threshold of $V_0$ [23]. Using fundamental measure density functional theory, we explicitly calculate the phase diagram in the plane spanned by $V_0$ and particle density for a fixed rod aspect ratio of 5. After having established the equilibrium behaviour, we consider an amplitude $V_0$ oscillating in time. A subtle resonance-like behaviour is detected for increasing oscillation frequencies if the oscillating $V_0$ crosses the paranematic–nematic phase boundary.

Our results can in principle be verified in real space [24] and scattering experiments [25] of rod-like colloidal suspensions. The external coupling can be realized by applying electric or magnetic fields [26, 27].

The paper is organized as follows: we recapitulate briefly the general fundamental measure theory for anisotropic hard bodies in section 2 and specialize it then to hard spherocylinders. The theory leaves a free parameter. In the same section 2, bulk properties of the isotropic and nematic phases are presented to fix the free parameter of the theory. In section 3 a static external aligning field is considered and the phase behaviour including a paranematic and nematic phase is computed. A time-dependent coupling is finally considered in section 4. We conclude in section 5.

## 2. Fundamental measure DFT for hard spherocylinders

### 2.1. General framework of edFMT

As for an equilibrium density functional for anisotropic hard bodies, we adopt the so-called 'extended deconvolution fundamental measure theory' (edFMT) which was recently proposed by Hansen-Goos and Mecke [16]. For a one-component system, the excess (i.e. over the ideal rotator) part of the Helmholtz free energy functional, $\mathcal{F}_{\rm exc}(T,[\rho])$, is written as

$$\mathcal{F}_{\rm exc}(T,V,[\rho^{(1)}]) = k_{\rm B}T\int_V {\rm d}^3r\,\Phi(\vec{r},[\rho^{(1)}]) \tag{1}$$

with $k_{\rm B}T$ denoting the thermal energy and $V$ the total volume of the system. Here the reduced excess free energy density $\Phi(\vec{r},[\rho])$ is

$$\Phi(\vec{r},[\rho]) = -n_0\ln(1-n_3) + \frac{n_1n_2 - \vec{n}_1\vec{n}_2 - \xi{\rm Tr}[\overleftrightarrow{n}_1\overleftrightarrow{n}_2]}{1-n_3} + \frac{3}{16\pi}\frac{\vec{n}_2^{\rm T}\overleftrightarrow{n}_2\vec{n}_2 - n_2\vec{n}_2\vec{n}_2 - {\rm Tr}[\overleftrightarrow{n}_2^3] + n_2{\rm Tr}[\overleftrightarrow{n}_2^2]}{(1-n_3)^2} \tag{2}$$

which involves a free parameter $\xi$ and a set of weighted densities $n_\alpha$. The latter are obtained by weighting the original density with weight functions $w_\alpha(\vec{r},\hat{\omega})$ such that

$$n_\alpha(\vec{r}) = \int_{S_2}{\rm d}^2\hat{\omega}'\int_V {\rm d}^3r'\,\rho^{(1)}(\vec{r}',\hat{\omega}')w_\alpha(\vec{r}-\vec{r}',\hat{\omega}'), \tag{3}$$

with $S_2$ denoting the surface of the unit sphere. The weight functions themselves are explicitly given by

$$w_0(\vec{r},\hat{\omega}) = \frac{K(\hat{r},\hat{\omega})}{4\pi}\cdot\delta(|\vec{R}(\hat{r},\hat{\omega})|-|\vec{r}|)\cdot\frac{1}{\hat{n}(\hat{r},\hat{\omega})\cdot\hat{r}} \tag{4}$$

$$w_1(\vec{r},\hat{\omega}) = \frac{H(\hat{r},\hat{\omega})}{4\pi}\cdot\delta(|\vec{R}(\hat{r},\hat{\omega})|-|\vec{r}|)\cdot\frac{1}{\hat{n}(\hat{r},\hat{\omega})\cdot\hat{r}} \tag{5}$$

$$w_2(\vec{r},\hat{\omega}) = \delta(|\vec{R}(\hat{r},\hat{\omega})|-|\vec{r}|)\cdot\frac{1}{\hat{n}(\hat{r},\hat{\omega})\cdot\hat{r}} \tag{6}$$

$$w_3(\vec{r},\hat{\omega}) = \Theta(|\vec{R}(\hat{r},\hat{\omega})|-|\vec{r}|) \tag{7}$$

$$\vec{w}_1(\vec{r},\hat{\omega}) = \frac{H(\hat{r},\hat{\omega})}{4\pi}\cdot\hat{n}(\hat{r},\hat{\omega})\cdot\delta(|\vec{R}(\hat{r},\hat{\omega})|-|\vec{r}|)\cdot\frac{1}{\hat{n}(\hat{r},\hat{\omega})\cdot\hat{r}} \tag{8}$$

$$\vec{w}_2(\vec{r},\hat{\omega}) = \hat{n}(\hat{r},\hat{\omega})\cdot\delta(|\vec{R}(\hat{r},\hat{\omega})|-|\vec{r}|)\cdot\frac{1}{\hat{n}(\hat{r},\hat{\omega})\cdot\hat{r}} \tag{9}$$

$$\overleftrightarrow{w}_1(\vec{r},\hat{\omega}) = (\vec{v}^{\rm I}(\hat{r},\hat{\omega})\cdot\vec{v}^{\rm I}(\hat{r},\hat{\omega})^{\rm T} - \vec{v}^{\rm II}(\hat{r},\hat{\omega})\cdot\vec{v}^{\rm II}(\hat{r},\hat{\omega})^{\rm T})\cdot\frac{\Delta\kappa(\hat{r},\hat{\omega})}{4\pi}\cdot\delta(|\vec{R}(\hat{r},\hat{\omega})|-|\vec{r}|)\cdot\frac{1}{\hat{n}(\hat{r},\hat{\omega})\cdot\hat{r}} \tag{10}$$

$$\overleftrightarrow{w}_2(\vec{r},\hat{\omega}) = \hat{n}(\hat{r},\hat{\omega})\cdot\hat{n}(\hat{r},\hat{\omega})^{\rm T}\cdot\delta(|\vec{R}(\hat{r},\hat{\omega})|-|\vec{r}|)\cdot\frac{1}{\hat{n}(\hat{r},\hat{\omega})\cdot\hat{r}}. \tag{11}$$

Here the following notations has been used. $\delta(x)$ and $\Theta(x)$ are the Dirac $\delta$-function and the Heaviside unit step function respectively. For a given shape $\mathcal{B}$ of a hard body characterized by its centre-of-mass $\vec{C}$ and orientation $\hat{\omega}$ (see figure 1), $\vec{R}(\hat{r},\hat{\omega})$ is parametrizing the body's surface, $\hat{n}(\hat{r},\hat{\omega})$ is the surface normal vector and $H(\hat{r},\hat{\omega})$ and $K(\hat{r},\hat{\omega})$ are the mean and Gaussian curvatures on the surface which are given in terms of the main curvatures $\kappa^{\rm I}(\hat{r},\hat{\omega})$ and $\kappa^{\rm II}(\hat{r},\hat{\omega})$ via $H(\hat{r},\hat{\omega}) = \frac{1}{2}(\kappa^{\rm I}(\hat{r},\hat{\omega}) + \kappa^{\rm II}(\hat{r},\hat{\omega}))$ and $K(\hat{r},\hat{\omega}) = \kappa^{\rm I}(\hat{r},\hat{\omega})\cdot\kappa^{\rm II}(\hat{r},\hat{\omega})$. Furthermore $\Delta\kappa(\hat{r},\hat{\omega}) = \frac{1}{2}(\kappa^{\rm I}(\hat{r},\hat{\omega}) - \kappa^{\rm II}(\hat{r},\hat{\omega}))$. $\vec{v}^{\rm I}(\hat{r},\hat{\omega})$ and $\vec{v}^{\rm II}(\hat{r},\hat{\omega})$ are the two directions of the main curvatures tangential to the surface. In equilibrium, for a given external potential $V_{\rm ext}(\vec{r},\hat{\omega})$, the one-particle density

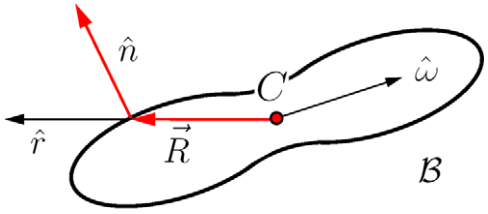


**Figure 1.** Parametrization of an anisotropic hard body of orientation characterized by a unit vector $\hat{\omega}$ and a centre-of-mass $C$. $\vec{R}$ points from $C$ towards the particle's surface and $\hat{r} = \vec{R}/|\vec{R}|$. $\hat{n}$ is the surface normal vector.

$\rho^{(1)}(\vec{r}, \hat{\omega})$ is given by minimizing the grandcanonical free energy functional $\Omega(T, V, \mu, [\rho])$, i.e.

$$\left.\frac{\delta\Omega(T, V, \mu, [\rho])}{\delta\rho(\vec{r}, \hat{\omega})}\right|_{\rho(\vec{r},\hat{\omega})=\rho^{(1)}(\vec{r},\hat{\omega})} = 0. \tag{12}$$

Here $\mu$ is the prescribed chemical potential. The functional $\Omega(T, V, \mu, [\rho])$ itself is decomposed as

$$\Omega(T, V, \mu, [\rho^{(1)}]) = \mathcal{F}(T, V, [\rho^{(1)}]) + \int_{S_2} \mathrm{d}^2\hat{\omega} \int_V \mathrm{d}^3 r\, \rho^{(1)}(\vec{r}, \hat{\omega})(V_{\mathrm{ext}}(\vec{r}, \hat{\omega}) - \mu) \tag{13}$$

with

$$\mathcal{F}(T, V, [\rho^{(1)}]) = \mathcal{F}_{\mathrm{id}}(T, V, [\rho^{(1)}]) + \mathcal{F}_{\mathrm{exc}}(T, V, [\rho^{(1)}]) \tag{14}$$

where

$$\mathcal{F}_{\mathrm{id}}(T, V, [\rho^{(1)}]) = k_{\mathrm{B}}T \times \int_{S_2} \mathrm{d}^2\hat{\omega} \int_V \mathrm{d}^3 r\, \rho^{(1)}(\vec{r}, \hat{\omega})[\ln(\rho^{(1)}(\vec{r}, \hat{\omega})\Lambda^3) - 1] \tag{15}$$

denotes the ideal gas functional of free rotators with $\Lambda$ being the (irrelevant) thermal de Broglie wavelength. Consequently, in (12), crucially the functional derivative $\frac{\delta\mathcal{F}_{\mathrm{exc}}(T,V,[\rho])}{\delta\rho}$ enters. Typically equation (12) is a nonlinear integral equation in $\rho^{(1)}(\vec{r}, \hat{\omega})$ which needs to be solved numerically.

### *2.2. Application of edFMT to orientational distributions of hard spherocylinders*

We now consider the special case of hard spherocylinders of aspect ratio $L/D$, see figure 2. In the following we assume throughout the paper that the one-particle density distribution $\rho^{(1)}(\vec{r}, \hat{\omega})$ solely depends on $\hat{\omega}$. Thereby we neglect smectic and other positionally-ordered phases but focus on isotropic, paranematic and nematic phases. Hence,

$$\rho^{(1)}(\vec{r}, \hat{\omega}) = \rho(\hat{\omega}) = \rho f(\hat{\omega}) \tag{16}$$

where $f(\hat{\omega})$ is normalized to one, $\int_{S_2} \mathrm{d}^2\hat{\omega} f(\hat{\omega}) = 1$. In this case the excess free energy functional simplifies and its functional derivative can be written as

$$\frac{\delta\mathcal{F}_{\mathrm{exc}}(T, V, [\rho])}{\delta\rho(\hat{\omega})} = k_{\mathrm{B}}T \sum_\alpha T_\alpha \cdot m_\alpha(\hat{\omega}) \tag{17}$$

with

$$m_\alpha(\hat{\omega}) = \int_V \mathrm{d}^3 r\, w_\alpha(\vec{r}, \hat{\omega}). \tag{18}$$

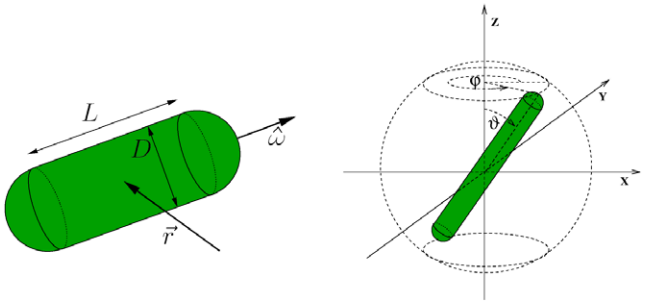


**Figure 2.** Hard spherocylinder of cylindrical length $L$ and diameter $D$ at centre-of-mass position $\vec{r}$ with orientation $\hat{\omega}$. Right: orientation of the spherocylinder on the unit sphere characterized by a polar angle $\varphi$ and an azimuthal angle $\vartheta$.

Moreover

$$T_0 = -\ln(1 - n_3) \tag{19}$$

$$T_1 = \frac{n_2}{1 - n_3} \tag{20}$$

$$T_2 = \frac{n_1}{1 - n_3} + \frac{3}{16\pi}\frac{\mathrm{Tr}(\overleftrightarrow{n}_2^2)}{(1 - n_3)^2} \tag{21}$$

$$T_3 = \frac{n_0}{1 - n_3} + \frac{n_1 n_2 - \xi \cdot \mathrm{Tr}(\overleftrightarrow{n}_1 \cdot \overleftrightarrow{n}_2)}{(1 - n_3)^2} + \frac{6}{16\pi}\frac{n_2\mathrm{Tr}(\overleftrightarrow{n}_2^2) - \mathrm{Tr}(\overleftrightarrow{n}_2^3)}{(1 - n_3)^3} \tag{22}$$

$$(\overleftrightarrow{T}_1)_{ij} = -\xi\frac{(\overleftrightarrow{n}_2)_{ij}}{1 - n_3} \tag{23}$$

$$(\overleftrightarrow{T}_2)_{ij} = \left[-\xi\frac{\overleftrightarrow{n}_1}{1 - n_3} - \frac{9}{16\pi}\frac{\overleftrightarrow{n}_2 \cdot \overleftrightarrow{n}_2}{(1 - n_3)^2} + \frac{6}{16\pi}\frac{n_2}{(1 - n_3)^2}\overleftrightarrow{n}_2\right]_{ij}, \tag{24}$$

where (3) with (18) reads

$$n_\alpha = \int_{S_2} \mathrm{d}^2\hat{\omega}\, \rho(\hat{\omega}) m_\alpha(\hat{\omega}) \tag{25}$$

and

$$m_0(\hat{\omega}) = 1 \tag{26}$$

$$m_1(\hat{\omega}) = \frac{L}{4} + \frac{D}{2} \tag{27}$$

$$m_2(\hat{\omega}) = \pi D(L + D) \tag{28}$$

$$m_3(\hat{\omega}) = \pi D^2\left(\frac{L}{4} + \frac{D}{6}\right) = v_{\mathrm{hsc}} \tag{29}$$

$$\vec{m}_1(\hat{\omega}) = \vec{0} \tag{30}$$

$$\vec{m}_2(\hat{\omega}) = \vec{0} \tag{31}$$

$$(\overleftrightarrow{m}_1)_{11}(\hat{\omega}) = \frac{L}{8}(1 + 3\cos^2(\varphi)\cos^2(\vartheta) - 3\cos^2(\varphi)) \tag{32}$$

$$(\overleftrightarrow{m}_1)_{22}(\hat{\omega}) = \frac{L}{8}(3\cos^2(\vartheta) - 3\cos^2(\varphi)\cos^2(\vartheta) - 2 + 3\cos^2(\varphi)) \tag{33}$$

$$(\overleftrightarrow{m}_1)_{33}(\hat{\omega}) = \frac{L}{8}(1 - 3\cos^2(\vartheta)) \tag{34}$$

$$(\overleftrightarrow{m}_1)_{21}(\hat{\omega}) = -\frac{3L}{8}\sin(\varphi)\cos(\varphi)\sin^2(\vartheta) \tag{35}$$

$$(\overleftrightarrow{m}_1)_{31}(\hat{\omega}) = -\frac{3L}{8}\cos(\varphi)\sin(\vartheta)\cos(\vartheta) \tag{36}$$

$$(\overleftrightarrow{m}_1)_{32}(\hat{\omega}) = -\frac{3L}{8}\sin(\varphi)\sin(\vartheta)\cos(\vartheta) \tag{37}$$

$$(\overleftrightarrow{m}_2)_{11}(\hat{\omega}) = \frac{\pi D}{6}(-3L\cos^2(\varphi) + 3L\cos^2(\varphi)\cos^2(\vartheta) + 3L + 2D) \tag{38}$$

$$(\overleftrightarrow{m}_2)_{22}(\hat{\omega}) = \frac{\pi D}{6}(3L\cos^2(\vartheta) - 3L\cos^2(\varphi)\cos^2(\vartheta) + 3L\cos^2(\varphi) + 2D) \tag{39}$$

$$(\overleftrightarrow{m}_2)_{33}(\hat{\omega}) = \frac{\pi D}{6}(3L - 3L\cos^2(\vartheta) + 2D) \tag{40}$$

$$(\overleftrightarrow{m}_2)_{21}(\hat{\omega}) = -\frac{\pi LD}{2}\sin(\varphi)\cos(\varphi)\sin^2(\vartheta) \tag{41}$$

$$(\overleftrightarrow{m}_2)_{31}(\hat{\omega}) = -\frac{\pi LD}{2}\cos(\varphi)\sin(\vartheta)\cos(\vartheta) \tag{42}$$

$$(\overleftrightarrow{m}_2)_{32}(\hat{\omega}) = -\frac{\pi LD}{2}\sin(\varphi)\sin(\vartheta)\cos(\vartheta), \tag{43}$$

where all tensorial parameters are symmetric.

### 2.3. Bulk isotropic–nematic transition

To calculate the equilibrium one-particle density $\rho(\hat{\omega})$ for a given chemical potential $\mu$ in a volume $V$, we use equations (12) and (13) to obtain the recursive conditional equation

$$\rho^{(1)}(\vec{r},\hat{\omega}) = \frac{1}{\Lambda^3}\cdot\exp\left\{\frac{\mu}{k_BT} - \frac{V_{ext}(\vec{r},\hat{\omega})}{k_BT} - \frac{1}{k_BT}\frac{\delta\mathcal{F}_{exc}(T,V,[\rho])}{\delta\rho(\vec{r},\hat{\omega})}\bigg|_{\rho(\vec{r},\hat{\omega})=\rho^{(1)}(\vec{r},\hat{\omega})}\right\}. \tag{44}$$

By iterating this equation (44), we obtain the equilibrium density (resp. orientational distribution) $\rho(\hat{\omega})$ that minimizes the grandcanonical free energy functional $\Omega[\rho]$, at least locally. This density $\rho(\hat{\omega})$ corresponds to a bulk equilibrium pressure $p$ which can be obtained as $p = -\Omega[\rho(\hat{\omega})]/V$. In the following we express the pressure in reduced units by defining the dimensionless reduced pressure $p^\star = pv_{hsc}/k_BT$ where $v_{hsc} = \pi D^2(\frac{L}{4} + \frac{D}{6})$ is the volume of a single spherocylinder. We further characterize orientational order using the dimensionless nematic order parameter $S$ which is defined as $S = \frac{3}{2}\lambda_S - \frac{1}{2}$, where $\lambda_S$ is the biggest eigenvalue of the nematic order parameter tensor

$$\overleftrightarrow{S} = \int_{S_2} f(\omega)\hat{\omega}\cdot\hat{\omega}^T\,d^2\hat{\omega}. \tag{45}$$

Its corresponding unit eigenvector $\hat{\lambda}_S$ is called the nematic director.

Varying the chemical potential $\mu$, we computed the equilibrium densities $\rho(\hat{\omega})$ for a fixed aspect ratio of $L/D = 5$ by starting the iteration from nematically pre-ordered densities $\rho_N(\hat{\omega})$ and ending in a nematic equilibrium density field. The integrals are solved numerically by using a static grid for the density field on the unit sphere with $128\times64$ equidistant points in spherical coordinates along the interval $[0\text{–}2\pi]\times[0\text{–}\pi]$.

On the other hand, we use isotropic densities $\rho_I(\hat{\omega}) =$ const as starting profiles. They stay constant and converge towards the equilibrium isotropic density. In figure 3(a) the difference between nematic and isotropic pressures is shown against the reduced chemical potential $\mu^\star = \mu/k_BT - 3\ln(\Lambda D^{-1})$ and it is obvious that nematic energies are lower than isotropic energies for $\mu^\star > \mu_c^\star$ resulting in isotropic–nematic coexistence at $\mu_c^\star = 19.852$. The corresponding reduced density defined as $\rho^\star = \rho/\rho_{cp}$, where $\rho_{cp}D^3 = \frac{2}{\sqrt{2}+\sqrt{3}L/D}$ is the close packing density, is plotted in figure 3(b) versus the reduced chemical potential. There is a small density jump of about 1% at coexistence showing that the isotropic–nematic transition is weakly first order. The nematic order parameter jumps from 0 to 0.41 at the transition as shown in figure 3(c). Finally in figure 3(d) the orientational dependence of the coexisting density profiles are shown.

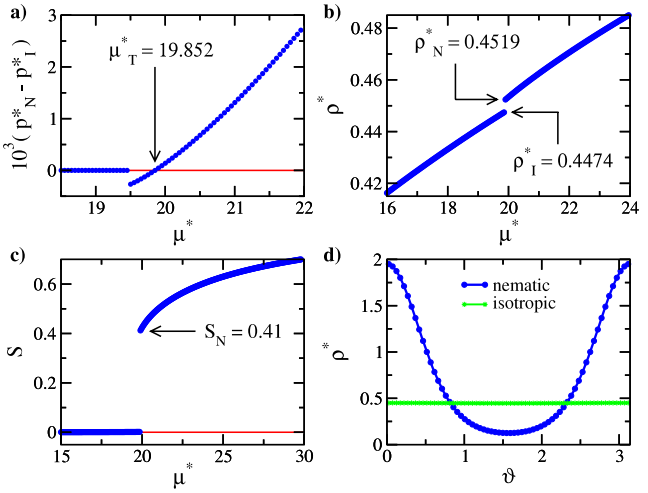


**Figure 3.** Several parameters describing the isotropic–nematic phase transition in a grandcanonical system of orientational hard spherocylinders with aspect ratio $L/D = 5$. For calculations edFMT with $\xi = 1.6$ has been used. (a) Reduced pressure difference between the nematic and isotropic phase versus the reduced chemical potential $\mu^\star = \mu/k_BT - 3\ln(\Lambda D^{-1})$. (b) Reduced mean density $\rho^\star = \rho/\rho_{cp}$ in the isotropic and nematic phase versus reduced chemical potential $\mu^\star$. (c) Nematic order parameter $S$ versus reduced chemical potential $\mu^\star$. (d) Orientational dependence of the density profile in the coexisting nematic and isotropic phase versus the azimuthal angle $\vartheta$ relative to the nematic director $\hat{\lambda}_S$. Coexistence occurs at $\mu_c^\star = 19.852$.

### 2.4. Comparison between theory and simulation

In the following, we compare bulk data of the edFMT theory with exact simulation results. The idea here is to get a feeling about the relevance and influence of the free parameter $\xi$ occurring in the edFMT theory.

In figure 4 the pressure difference and the nematic order parameter are shown versus the reduced chemical potential as in 3(a) and (c) but now for different parameters $\xi$. The vertical line indicates the exact transition point at $\mu^\star = 21.772$ according to computer simulations [9, 28]. From this one can already conclude that a $\xi$ value of about 1.5–1.6 fits the exact data best as the data for $\xi = 1.5$ and 1.6 bracket the simulation data.

For various aspect ratios $L/D$ a comparison of the coexistence pressures is shown in figure 5. Here slightly higher

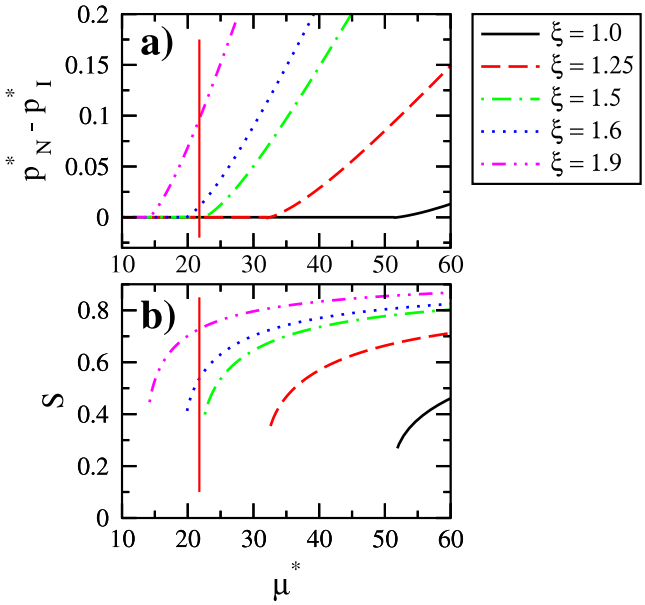


**Figure 4.** Same as in figures 3(a) and (c) but now for different parameters $\xi$. The vertical line marks the simulation data of [9, 28] for the isotropic nematic transition point where $\mu^\star = 21.772$, $p^\star = 5.30$, $\rho^\star_I = 0.461$ and $\rho^\star_N = 0.470$. edFMT predicts the following transition points: for $\xi = 1.0$: $\mu^\star = 51.904$, for $\xi = 1.25$: $\mu^\star = 32.506$, for $\xi = 1.5$: $\mu^\star = 22.536$, for $\xi = 1.6$: $\mu^\star = 19.844$ and for $\xi = 1.9$: $\mu^\star = 14.150$.

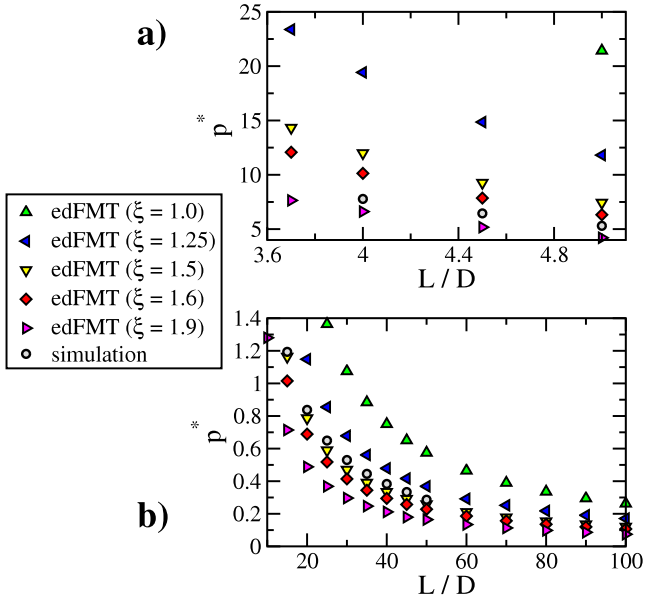


**Figure 5.** Reduced pressure at isotropic–nematic coexistence versus the aspect ratio $L/D$ of the spherocylinders for various values of the parameter $\xi$. Simulation data were taken from [28] (a) and [9] (b). Figures (a) and (b) show different ranges in the aspect ratio $L/D$.

values for $\xi$ would give a better fit, but still $\xi = 1.6$ is a reasonable choice.

The next comparison concerns the density jump across the isotropic–nematic transition in figure 6 as it has been done in [16]. Here it is obvious that edFMT underestimates the size of the jump, but is in fair agreement with its position.

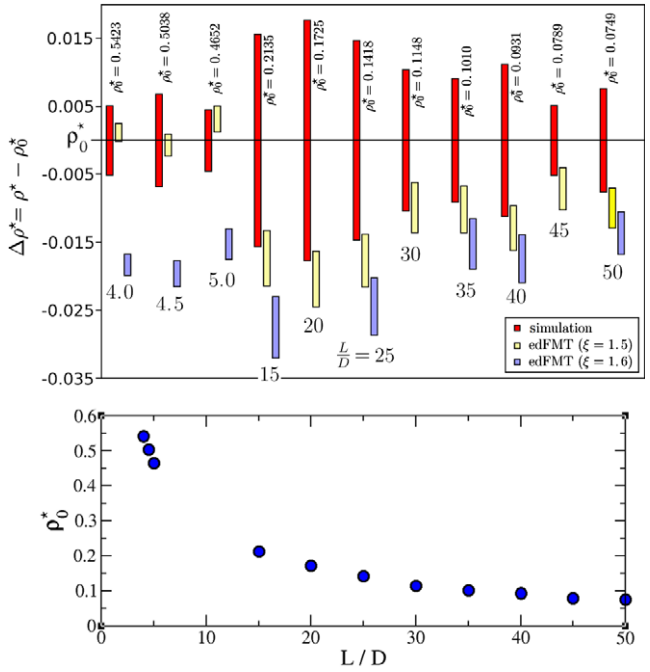


**Figure 6.** Size and position of the density jump at the isotropic nematic transition point versus aspect ratio $L/D$, written below the bars. These bars are showing the size of the density jump and its position relative to a chosen value $\rho_0 = \frac{1}{2}(\rho_I + \rho_N)$ as centre of the density jump in simulations, written above the bars and shown in the second graph. Simulation data were taken from [28] for $L/D \geqslant 5$ and from [9] otherwise.

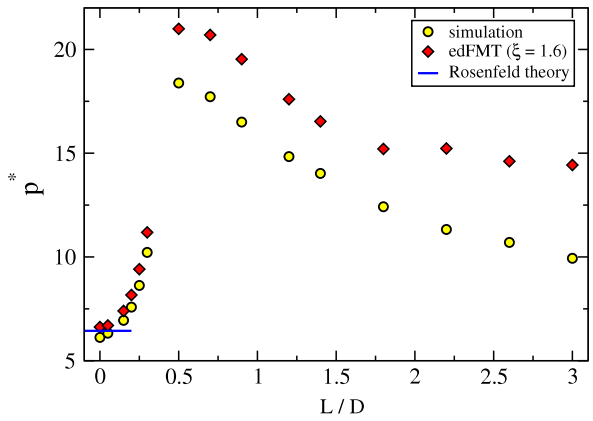


**Figure 7.** Pressure at the isotropic/plastic crystal coexistence. The isotropic densities $\rho^\star_I$ at coexistence are taken from [9].

Interestingly, edFMT's pressures are also in good agreement with simulations for high densities. Finally, in figure 7 pressures of the isotropic phase at coexistence with the plastic crystal are shown at low aspect ratios. For $\xi = 1.6$ there is good agreement with the simulation data [9]. In case of spherical particles for $L/D = 0$ these data are compared to Rosenfeld's FMT [13, 14] which is the natural reduction of edFMT in the limit of spherical particles.

edFMT does not reproduce the Onsager limit [29] of infinitely thin rods, $L/D \to \infty$, on the level of the functional, but gives nevertheless reasonable data for the isotropic nematic

**Table 1.** Comparison between edFMT data and Onsager theory [29] for the coexisting isotropic density at the isotropic–nematic transition. The ratio between the Onsager and the edFMT expression is denoted by $\Delta$. This ratio has been averaged over an aspect ratio interval $L/D \in [100; 600]$ with a maximal variance which is also given as the error.

| $\xi$ | 1.0 | 1.25 | 1.5 | 1.6 | 1.9 |
|---|---|---|---|---|---|
| $\Delta$ | $0.768 \pm 0.011$ | $0.965 \pm 0.02$ | $1.15 \pm 0.017$ | $1.255 \pm 0.03$ | $1.52 \pm 0.05$ |

transition. For instance, the number density of the coexisting isotropic phase is analytically given in the Onsager limit as $\frac{13.16}{\pi L^2 D}$. The ratio of this density with that obtained from edFMT can be averaged over an aspect ratio interval $L/D \in [100; 600]$. The resulting average $\Delta$ is shown for different $\xi$ in table 1. Obviously, in the Onsager limit $\xi = 1.25$ is a better choice consistent with what was found in [16, 30].

In the following we shall concentrate on a rod aspect ratio of 5. We shall therefore keep the parameter $\xi$ fixed to 1.6. However, if longer rods are considered, clearly smaller values for $\xi$ should be used.

## 3. Paranematic–nematic transition in a static external aligning field

Now we introduce an external aligning field

$$V_{\text{ext}}(\hat{\omega}) = -V_0 \cdot \sin^2(\vartheta) \tag{46}$$

that depends only on the particle orientations. With positive prefactor $V_0$, this potential forces the orientation of particles to be within the $xy$-plane, away from the $z$-axis which is the reference axis for the azimuthal angle $\vartheta$. On the other hand, a negative field strength $V_0 < 0$ causes a potential that forces the orientations to be along the $z$-axis, away from the $xy$-plane. As a remark, since $\sin^2 = -\cos^2 + 1$, apart from a trivial additive constant, the potential $V_{\text{ext}}(\hat{\omega})$ is equivalent to $V_0 \cdot \cos^2(\vartheta)$ which is sometimes a more convenient expression in the literature.

In the low density limit, the external field causes an isotropic system to develop a nontrivial orientational distribution, so that for nonzero field strength $V_0 \neq 0$ isotropic phases get orientational order and are therefore called paranematic.

The edFMT density functional is used to calculate the phase diagram for hard spherocylinders (with fixed $\xi = 1.6$) in the external field. The functional is minimized in the grandcanonical ensemble at a prescribed chemical potential $\mu$ and temperature $T$. Coexistence of paranematic and nematic phases is identified by searching for two orientational distributions with the same grandcanonical free energy density (corresponding to equal pressure). The corresponding coexisting densities are plotted in figure 8 for fixed aspect ratio $L/D = 5$ and varied aligning strength $V_0$.

For $V_0 > 0$, shown in figure 8(b), we found a critical endpoint at $V_0 \approx 0.35 k_B T$ in accordance to the finding of Wensink and Vroege [23]. Below this point the transition is first order, above, i.e. for $V_0 > 0.35 k_B T$, it is second order. In both situations, the transition is characterized by spontaneous orientational order on the *equator* of the unit sphere. In the paranematic phase, the orientations are uniformly distributed along the equator, i.e. the density profile $\rho(\hat{\omega}) = \rho(\vartheta)$ does

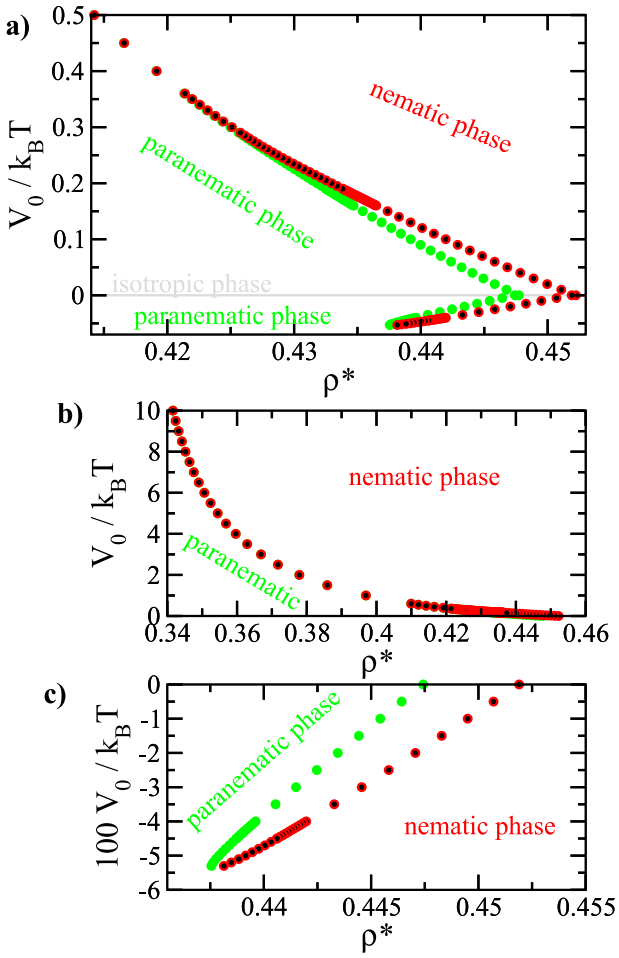


**Figure 8.** Phase diagram with the external potential (46) for an aspect ratio $L/D = 5$. Shown are the densities at the transition line in the isotropic/paranematic phase and in the nematic phase. The critical endpoint is at $V_0 \approx 0.35 k_B T$, $\rho^\star \approx 0.4219 \pm 0.0001$ and the threshold point below which there is no transitions at all lies at $V_0 \approx -0.054 k_B T$ and $\rho^\star \approx 0.4378 \pm 0.0004$. (b) and (c) are the same data on a larger scale for positive and negative $V_0$ respectively.

not depend on the polar angle $\varphi$. In the nematic phase, on the other hand, there is an orientational peak along the equator in the (reduced) profile with a maximum $\rho^\star_{\text{max}}$. Therefore the paranematic–nematic transition can be characterized by an order parameter that measures the equatorial inhomogeneity of the density profile. Accordingly, we define an equatorial nematic order parameter $S_{\text{eq}}$ which is related to the first non-vanishing Fourier coefficient in an expansion of the orientational profile along the equator with respect to the polar angle $\varphi$ for fixed $\vartheta = \pi/2$. In detail, we define

$$S_{\text{eq}} = \sqrt{c^2 + d^2} \tag{47}$$

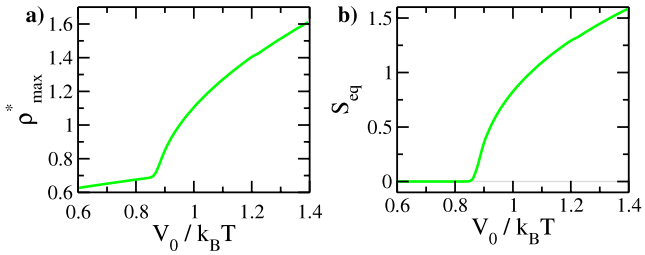


**Figure 9.** Peak amplitude $\rho^\star_{\max}$ of the equatorial density field (a) and equatorial nematic order parameter $S_{\rm eq}$ (b) versus aligning field amplitude $V_0$ at fixed density $\rho^\star = 0.4$. The second-order paranematic–nematic transition occurs at $V_0 \approx 0.87 k_{\rm B}T$. The further parameters are $L/D = 5$ and $\xi = 1.6$.

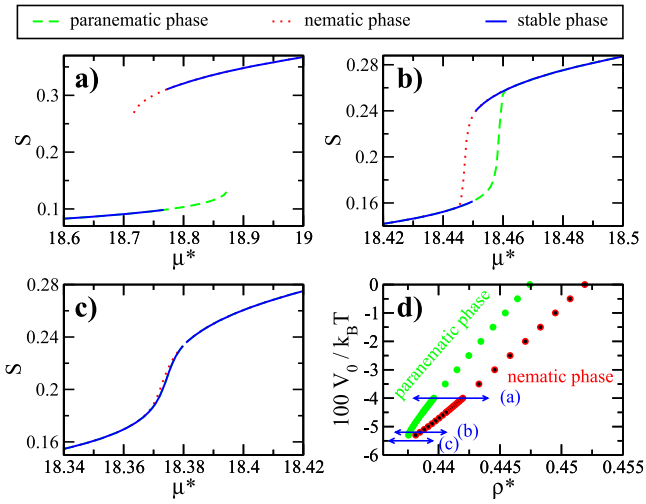


**Figure 10.** Nematic order parameter $S$ at the isotropic/paranematic to nematic transition in orientable hard spherocylinders with aspect ratio $L/D = 5$ in an aligning external potential at different negative field strengths $V_0$ ((a)–(c)) versus the reduced chemical potential: (a) $V_0 = -0.04 k_{\rm B}T$, (b) $V_0 = -0.052 k_{\rm B}T$, (c) $V_0 = -0.055 k_{\rm B}T$. These different values for $V_0$ are plotted in the $V_0$–density plane in (d). The reduced chemical potential at the phase transition is $\mu^\star = 18.7691$ (a) and $\mu^\star \approx 18.4505$ (b).

with the coefficients

$$c = \frac{1}{\pi\rho^\star}\int_0^{2\pi} \sin(2\varphi)\rho^\star\left(\varphi, \frac{\pi}{2}\right) \mathrm{d}\varphi \qquad (48)$$

$$d = \frac{1}{\pi\rho^\star}\int_0^{2\pi} \cos(2\varphi)\rho^\star\left(\varphi, \frac{\pi}{2}\right) \mathrm{d}\varphi. \qquad (49)$$

In figure 9, both $\rho^\star_{\max}$ and $S_{\rm eq}$ are shown for fixed overall density $\rho^\star = 0.4$. The range of alignment strength considered is sketched as a double arrow in figure 11. In fact, at about $V_0 \approx 0.87 k_{\rm B}T$, the order parameter $S_{\rm eq}$ levels off from zero continuously indicating the second-order paranematic–nematic transition. Likewise the density peak $\rho^\star_{\max}$ exhibits a second-order nonanalyticity at the transition.

For $V_0 < 0$, shown in figure 8(c), there is a threshold strength below which no transition exists at all, as known from earlier investigations [8, 22, 23]. This produces a 'finger' in the coexistence densities. For our parameters, the threshold

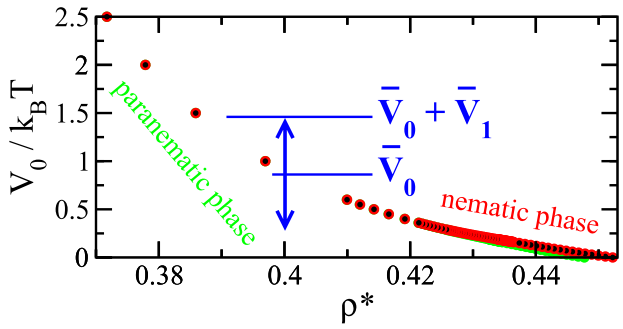


**Figure 11.** Range of the time-dependent amplitude $V_0$ shown as a path (arrow) in the equilibrium phase diagram of figure 8. The parameters are $L/D = 5$, $\rho^\star = 0.4$, $\xi = 1.6$. The transition point for the mean density $\rho^\star = 0.4$ is at $V_0 \approx 0.875 k_{\rm B}T$.

strength is about $-0.055 k_{\rm B}T$. Clearly there is no $V_0 \to -V_0$ symmetry due to the different topology of the two regions on the unit sphere (equator and pole) which are preferred by the aligning field. More details across the paranematic–nematic transition at various negative field strengths are contained in figure 10 where the nematic order parameter $S$ is shown across the transition (a) and (b) and below the threshold strength (c).

In section 4 the external coupling $V_0$ is made time dependent. The equilibrium phase diagram discussed here therefore serves as a reference situation for very slow time dependencies where the relaxed system will follow the instantaneous equilibrium situation.

## 4. Dynamical density functional theory

### *4.1. Theoretical framework*

For Brownian rods, the equilibrium density functional theory can be generalized towards nonequilibrium dynamics, generated e.g. by time-dependent external potentials. This leads to so-called dynamical density functional theory (DDFT) which can be derived from the Smoluchowski equation [17] with the only approximation that the one-particle density evolves much slower than any other higher-order correlation function. DDFT first was considered for spherical interactions but was recently generalized to both translational and orientational degrees of freedom [20]. As a result, there is a deterministic evolution equation for the time-dependent one-particle density which can be understood as a generalized continuity equation conserving the overall density. If the one-particle density solely depends on the orientations, the dynamical equation reads as follows [20]:

$$k_{\rm B}T\frac{\partial\rho(\hat{\omega},t)}{\partial t} = D_{\rm r}\hat{R}\cdot\left[\rho(\hat{\omega},t)\hat{R}\frac{\delta\Omega[\rho(\hat{\omega}',t)]}{\delta\rho(\hat{\omega},t)}\right], \qquad (50)$$

where $D_{\rm r}$ is the rotational diffusion coefficient of the Brownian rods which sets the timescale $\tau_{\rm B} = 1/D_{\rm r}$ and $\hat{R} = \hat{\omega} \times \bar{\nabla}_{\hat{\omega}}$ is the rotational gradient operator[1]. In the following,

[1] As a remark, one could also take the Helmholtz free energy functional on the right-hand side of equation (50) which leads to exactly the same equation of motion.

we use edFMT to describe the density functional input for hard spherocylinders and consider an external time-dependent aligning field $V_{\rm ext}(\hat{\omega}, t)$. The equation (50) is then solved by a straightforward numerical finite difference method with respect to time involving typically $10^8$ time steps $\Delta t = 5 \times 10^{-5}\tau_{\rm B}$.

### 4.2. Results for an oscillating external aligning potential

We now apply the dynamical theory to an orientationally inhomogeneous fluid of hard spherocylinders. In doing so, we prescribe the mean density $\rho^\star = 0.4$. This density will be time independent as it is conserved. A time-dependent external potential is applied in which the aligning amplitude $V_0$ depends on time $t$. We chose a harmonic variation with an external shaking frequency $\bar{\omega}$:

$$V_0(t) = \bar{V}_0 + \bar{V}_1 \cdot \cos(\bar{\omega} \cdot t) \tag{51}$$

such that the total external potential becomes

$$V_{\rm ext}(\hat{\omega}, t) = -V_0(t) \cdot \sin^2(\vartheta). \tag{52}$$

Here $\bar{V}_0$ is the mean (or time-averaged) amplitude. For any fixed time, the situation corresponds to a point in the $\rho^\star V_0$ plane of the equilibrium phase diagram. Formally one can therefore represent the time dependence in $V_0(t)$ as a path in this phase diagram. However, it is only for very slow variation in $V_0(t)$ that the actual state is in equilibrium. This path in the $\rho^\star V_0$ plane is schematically shown in figure 11.

Starting from an equilibrated density profile at $V_0 = \bar{V}_0 + \bar{V}_1$ the system relaxes towards an oscillatory nonequilibrium steady state. Properties of this oscillatory steady state are presented in figure 12 for two different shaking frequencies $\bar{\omega}$ and the 'adiabatic' limit $\hat{\omega} \to 0^+$. The response of the density field to the external shaking is characterized by the time-dependent peak amplitude $\rho^\star_{\rm max}$ of the orientational order along the equator and the equatorial nematic order parameter $S_{\rm eq}$, see 12(b) and (c). While the response is mainly harmonic in time for the larger frequencies, anharmonicities are clearly visible for the smaller frequency. This has to do with dynamical asymmetries in the paranematic and nematic phase which are touched along the periodic oscillation and fully show up in the limit $\hat{\omega} \to 0^+$. As is revealed by figure 12, both nonzero frequencies considered here ($\hat{\omega}\tau_{\rm B}/2\pi = 0.01, 0.1$) are significantly off from the adiabatic limit $\hat{\omega} \to 0^+$. As typical for overdamped systems there is a phase shift of the response relative to the drive.

The relaxation into the oscillatory steady state is explored in figure 13 for a fixed frequency $\bar{\omega}\tau_{\rm B}/2\pi = 1$ and $\bar{V}_0 = 0.88 k_{\rm B}T$ and various $\bar{V}_1$. For $\bar{V}_1/k_{\rm B}T$ being the range of 0–0.5, the relaxation behaviour—as revealed in the time dependencies of the equatorial peak amplitude $\rho^\star_{\rm max}(t) = \max_{\hat{\omega}} \rho(\hat{\omega}, t)$ and the equatorial nematic order parameter $S_{\rm eq}$—is shown for 300 cycles in figure 13(a). Even after this long periodic external driving, the system is still a little bit away from its final steady state as signalled by long-time tail apparent in figure 13(a). Most data were obtained for 300 cycles but we checked longer cycles as well. As a result, fortunately,

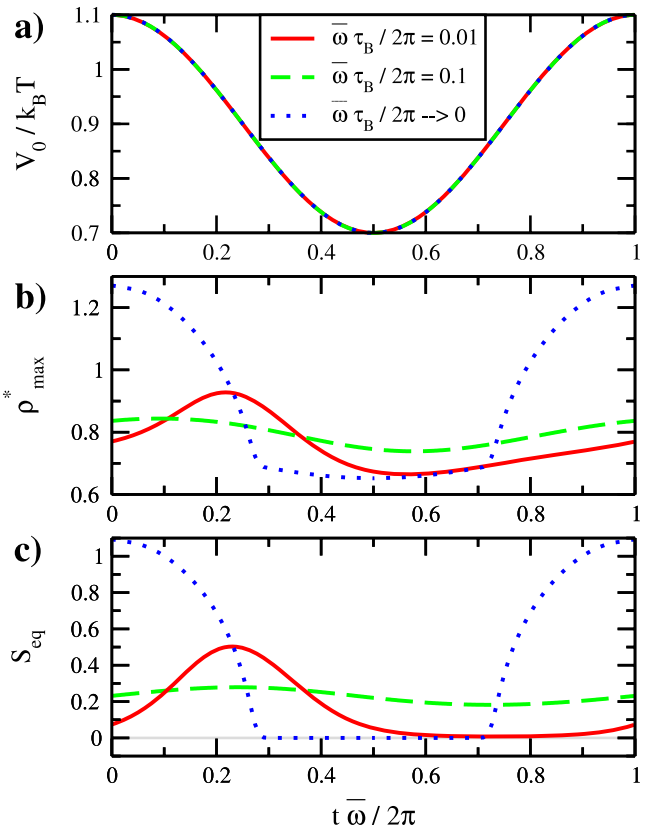


**Figure 12.** Oscillation cycle in the steady state for the frequencies $\bar{\omega}\tau_{\rm B}/2\pi = 0^+, 0.1, 0.01$. The harmonic time dependency of the aligning amplitude $V_0(t)$ is shown in (a) with $\bar{V}_0 = 0.9 k_{\rm B}T$. The peak maximum $\rho^\star_{\rm max}$ and the equatorial order parameter $S_{\rm eq}$ are presented in (b) and (c).

one has to be careful for long-time corrections only when $\bar{V}_0/k_{\rm B}T < 0.92$. Moreover, qualitative trends are not affected at all by these corrections. In addition, $\rho^\star_{\rm max}$ is plotted on a finer resolution as a function of time in 13(c) for various $\bar{V}_1$ which resolves the band shown in (a).

Ignoring the small long-time corrections, we show in figure 14 the dependence of the time-averaged equatorial nematic order parameter $\langle S_{\rm eq}\rangle$ in the steady state as a function of $\bar{V}_0$ for various $\bar{V}_1$. Clearly $\langle S_{\rm eq}\rangle$ increases with increasing $\bar{V}_0$, while the trend with varied oscillation amplitude $\bar{V}_1$ is a bit less obvious. Increasing $\bar{V}_1$, leads to larger excursions in the $V_0\rho^\star$ plane. Delving deeper into the paranematic region will not change $S_{\rm eq}$ since it vanishes there anyway while exploring the nematic region more will lead to an increase of equatorial nematic order. Therefore $\langle S_{\rm eq}\rangle$ rises with increasing $\bar{V}_1$, too. Strikingly, the nonequilibrium steady-state transition seems to be again second order and shifts to larger aligning amplitudes $V_0$ relative to the equilibrium transition (solid line in figure 14). This can be intuitively understood by the argument that shaking leads to more disorder and hence a stronger aligning force is needed for the transition. A similar effect was seen for freezing in shaken solids in [31].

Finally, we study the response as a function of the external oscillation frequency $\bar{\omega}$. The maximal peak amplitude $\max_t(\max_\varphi \rho(\varphi, \pi/2, t))$, the minimal peak

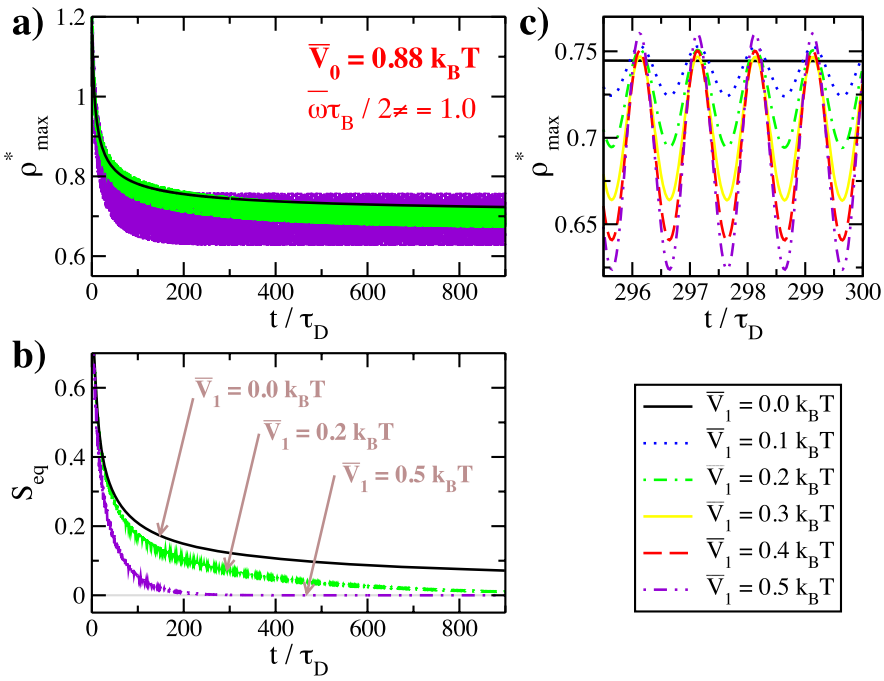


**Figure 13.** Relaxation from an equilibrated nematic profile with $S = 0.26$ to the steady state for $\bar{\omega}\tau_B/2\pi = 1$ and $\bar{V}_0 = 0.88 k_B T$. Equatorial peak amplitude $\rho^\star_{max}$ (a) and equatorial nematic order parameter $S_{eq}$ (b) versus time during 900 oscillation periods for various $\bar{V}_1$ as indicated in the inset, (c) $\rho^\star_{max}$ versus time after 296 cycles (same as (a)) but on a finer scale.

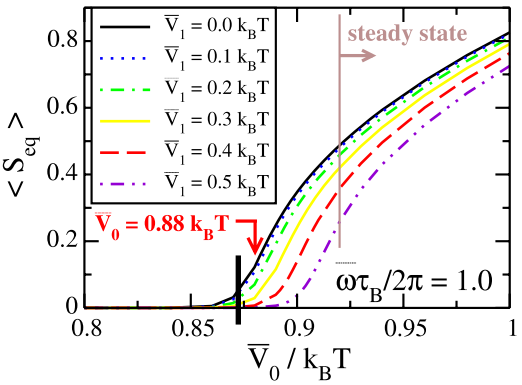


**Figure 14.** Time-averaged equatorial order parameter $\langle S_{eq}\rangle$ in the steady state, i.e. after 300 cycles for fixed $\bar{\omega}\tau_B/2\pi = 1$ as a function of $\bar{V}_0$ for various $\bar{V}_1$ as indicated in the legend. The value used in the preceding figure is indicated by an arrow. The location of the equilibrium second-order transition is approximately marked by a bar including a long-time relaxation correction. If the cycle number goes to infinity the data shift a bit to the right. The long-time corrections are irrelevant for $\bar{V}_0 \geqslant 0.92 k_B T$ and for $\bar{V}_0 \lessapprox 0.85 k_B T$.

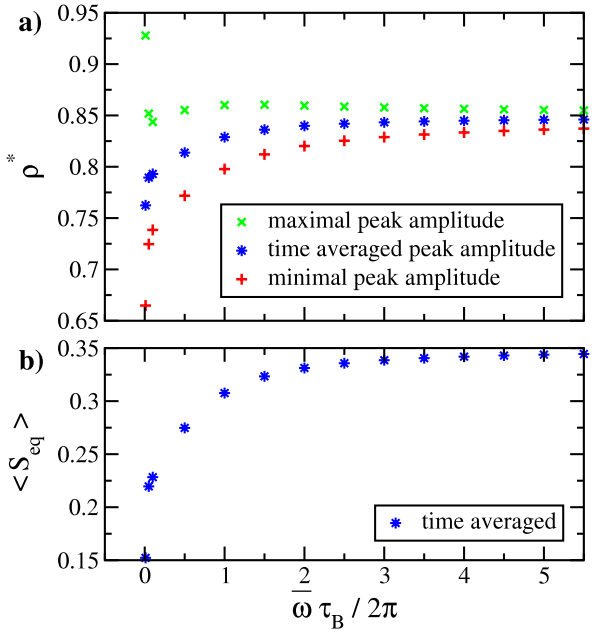


**Figure 15.** Maximal peak amplitude, time-averaged peak amplitude and minimal peak amplitude (a) as well as the time-averaged equatorial order parameter $\langle S_{eq}\rangle$ (b) versus external frequency $\bar{\omega}\tau_B$ after a time of $180\tau_B$ ($500\tau_B$ for $\bar{\omega}\tau_B/2\pi \leqslant 0.1$). The further parameters are $L/D = 5$, $\rho^\star = 0.4$, $\bar{V}_0 = 0.9 k_B T$ and $\bar{V}_1 = 0.2 k_B T$.

amplitude $\min_t(\max_\varphi \rho(\varphi, \pi/2, t))$ and the time average peak amplitude $\int_T^{T+2\pi/\bar{\omega}} \mathrm{d}t\,(\max_\varphi \rho(\varphi, \pi/2, t))$ are plotted in the steady state as a function of $\bar{\omega}$ in figure 15. Here $T \gg \tau_B$ is a large time ensuring full relaxation into the steady state. The two extreme limit can be easily understood first: for very large frequencies $\bar{\omega} \to \infty$ this is a static equilibrium situation with $V_0 = \bar{V}_0$ where there is no time oscillation. Therefore the maximal and the minimal peak amplitude coincide and the equatorial order parameter saturates to its corresponding static value. The second opposite limit is $\bar{\omega} \to 0^+$ which is different from the case $\bar{\omega} = 0$ where everything is a priori static, see equation (51). In fact, for $\bar{\omega} = 0$ we get from figure 9 the values $\rho^\star_{max} = 1.271$ and $S_{eq} = 1.093$ at $V_0(0) = 1.1 k_B T$. These data are different from those plotted in figure 15, where,

for $\bar{\omega} \to 0^+$ we expect an 'adiabatic' response described by the equilibrium phase diagram. In between, a *resonance* pops up as visible in a weak secondary maximum at $\bar{\omega}\tau_B = 6$ for the maximal peak amplitude. This possibly reveals an asymmetry of relaxation dynamics in the paranematic and nematic phase but its detailed origin is still unclear. In fact, the resonance is subtle since it does not occur in the difference between the maximal and minimal peak amplitude. Nevertheless it is unusual for completely overdamped Brownian dynamics.

## 5. Conclusions

In conclusion, we have applied the fundamental measure density functional for hard spherocylinders, proposed recently by Hansen-Goos and Mecke [16], to equilibrium situations and nonequilibrium dynamics. For the latter, we used the framework of dynamical density functional theory for orientable bodies. In particular, an external field was applied which only couples to the orientations of the particles. First, the static phase behaviour was computed involving paranematic and nematic phases. The topology of the paranematic–nematic phase behaviour in the plane spanned by the density and aligning field strength is different if the rods are preferentially oriented towards the poles or the equator of a unit sphere. In the former case (alignment along the poles) the transition is first order but vanishes above a critical amplitude. In the latter it changes from first to second order but is persistent at any coupling strength. If the aligning field amplitude is oscillatory in time, scanning the static phase diagram, there is a resonance effect for increasing driving frequency.

Our results can be realized in experiments on rod-like colloids in aligning external fields [24, 25, 32]. For future studies it would be interesting to relax the essential constraint that the full one-particle density does not depend on the translational position. Though numerically more complicated, this would be a promising route towards the full equilibrium phase behaviour which involves various liquid crystalline phases like a plastic crystal, smectic layering and full crystalline ordering [9]. Once the coexisting phases are identified, their interfaces can also be accessed using density functional theory [33]. For instance,the structure of the isotropic–nematic [34–36] and the nematic–smectic [37] interface can be computed and the corresponding interfacial free energy can be extracted. Furthermore the tagged particle dynamics [19, 38] can in principle be studied in equilibrium by generalizing the idea of Archer, Hopkins and Schmidt [39] towards orientational degrees of freedom.

Nonequilibrium dynamics is expected to become even more complex. In particular, regarding the smectic phases, unusual features have been detected in its homogeneous nucleation behaviour [40, 41]. Heterogeneous nucleation at imposed nucleation clusters [42] and behaviour of rods in time-dependent confining traps [43] is expected to bear many more fascinating effects which are yet unexplored. These can in principle be addressed using the dynamical theory proposed in this paper.

## Acknowledgments

We thank R Blaak and H H Wensink for helpful discussions. Financial support is acknowledged from the DFG within SFB TR6 (project D3) and SPP 1296.

## References

[1] Evans R 1979 *Adv. Phys.* **28** 143
[2] Singh Y 1991 *Phys. Rep.* **207** 351
[3] Oxtoby D W 1991 *Liquids, Freezing and the Glass Transition* (*Les Houches Summer Schools of Theoretical Physics Session LI (1989)* vol Session LI (1989)) (Amsterdam: Springer North Holland) chapter 3, p 147
[4] Oxtoby D W 2000 *Nature* **406** 464
[5] Löwen H 1994 *Phys. Rep.* **237** 249
[6] Tarazona P, Cuesta J A and Martínez-Ratón Y 2008 *Theory and Simulation of Hard-Sphere Fluids and Related Systems* (*Springer Lecture Notes in Physics*) vol 753 (Berlin: Springer) chapter 7, pp 247–341
[7] Poniewierski A and Holyst R 1988 *Phys. Rev. Lett.* **61** 2461
[8] Graf H and Löwen H 1999 *J. Phys.: Condens. Matter* **11** 1435
[9] Bolhuis P and Frenkel D 1997 *J. Chem. Phys.* **106** 666
[10] Graf H, Löwen H and Schmidt M 1997 *Prog. Colloid Polym. Sci.* **104** 177
[11] Graf H and Löwen H 1999 *Phys. Rev.* E **59** 1932
[12] Frenkel D 1991 *Liquids, Freezing and the Glass Transition* (*Les Houches Summer Schools of Theoretical Physics Session LI (1989)* vol Session LI (1989)) ed J P Hansen, D Levesque and J Zinn-Justin (Amsterdam: Springer North Holland) chapter 9, pp 689–756
[13] Rosenfeld Y 1989 *Phys. Rev. Lett.* **63** 980
[14] Rosenfeld Y, Schmidt M, Löwen H and Tarazona P 1997 *Phys. Rev.* E **55** 4245
[15] Roth R, Evans R, Lang A and Kahl G 2002 *J. Phys.: Condens. Matter* **14** 12063
[16] Hansen-Goos H and Mecke K 2009 *Phys. Rev. Lett.* **102** 018302
[17] Archer A J and Evans R 2004 *J. Chem. Phys.* **121** 4246
[18] Dhont J K G 1996 *An Introduction to Dynamics of Colloids* (Amsterdam: Elsevier)
[19] Löwen H 1994 *Phys. Rev.* E **50** 1232
[20] Rex M, Wensink H H and Löwen H 2007 *Phys. Rev.* E **76** 021403
[21] Wensink H H and Löwen H 2008 *Phys. Rev.* E **78** 031409
[22] Khokhlov A R and Semenov A N 1982 *Macromolecules* **15** 1272
[23] Wensink H H and Vroege G J 2005 *Phys. Rev.* E **72** 031708
[24] Kang K and Dhont J K G 2008 *Europhys. Lett.* **84** 14005
[25] Wandersman E, Dubois E, Cousin F, Dupuis V, Meriguet G, Perzynski R and Cebers A 2009 *Europhys. Lett.* **86** 10005
[26] Löwen H 2001 *J. Phys.: Condens. Matter* **13** R415
[27] van der Beek D, Davidson P, Wensink H H, Vroege G J and Lekkerkerker H N W 2008 *Phys. Rev.* E **77** 031708
[28] McGrother S C, Williamson D C and Jackson G 1996 *J. Chem. Phys.* **104** 6755
[29] Onsager L 1949 *Ann. New York Acad. Sci.* **51** 627
[30] Hansen-Goos H 2008 *PhD Thesis* Fakultät für Mathematik und Physik der Universität Stuttgart
[31] Löwen H and Hoffmann G P 1999 *Phys. Rev.* E **60** 3009
[32] MacKenzie K R and McKay G 2004 *Mol. Cryst. Liq. Cryst.* **413** 197
[33] Ohnesorge R, Löwen H and Wagner H 1994 *Phys. Rev.* E **50** 4801
[34] Akino N, Schmid F and Allen M P 2001 *Phys. Rev.* E **63** 041706

[35] van der Beek D, Reich H, van der Schoot P, Dijkstra M, Schilling T, Vink R, Schmidt M, van Roij R and Lekkerkerker H 2006 *Phys. Rev. Lett.* **97** 087801
[36] McDonald A J, Allen M P and Schmid F 2000 *Phys. Rev.* E **63** 010701
[37] Grelet E, Lettinga M P, Bier M, van Roij R and van der Schoot P 2008 *J. Phys.: Condens. Matter* **20** 494213
[38] Löwen H 1999 *Phys. Rev.* E **59** 1989
[39] Archer A J, Hopkins P and Schmidt M 2007 *Phys. Rev.* E **75** 040501
[40] Schilling T and Frenkel D 2004 *Phys. Rev. Lett.* **92** 085505
[41] Cuetos A, van Roij R and Dijkstra M 2008 *Soft Matter* **4** 757
[42] van Teeffelen S, Likos C N and Löwen H 2008 *Phys. Rev. Lett.* **100** 108302
[43] Rex M and Löwen H 2008 *Phys. Rev. Lett.* **101** 148302